Structures of aminoacylase 3 in complex with acetylated substrates

Jennifer M. Hsieh[a,b,1], Kirill Tsirulnikov[c,1], Michael R. Sawaya[d], Nathaniel Magilnick[c], Natalia Abuladze[c], Ira Kurtz[c], Jeff Abramson[b,2], and Alexander Pushkin[c,2]

[a]Department of Chemistry and Biochemistry, University of California, Los Angeles, CA 90095; [b]Departments of Physiology and [c]Medicine/Nephrology, David Geffen School of Medicine at University of California, Los Angeles, CA 90095; and [d]Howard Hughes Medical Institute, University of California–Department of Energy Institute for Genomics and Proteomics, Los Angeles, CA 90095

Edited* by George H. Lorimer, University of Maryland, College Park, MD, and approved August 24, 2010 (received for review June 2, 2010)

Trichloroethylene (TCE) is one of the most widespread environmental contaminants, which is metabolized to *N*-acetyl-*S*-1,2-dichlorovinyl-L-cysteine (NA-DCVC) before being excreted in the urine. Alternatively, NA-DCVC can be deacetylated by aminoacylase 3 (AA3), an enzyme that is highly expressed in the kidney, liver, and brain. NA-DCVC deacetylation initiates the transformation into toxic products that ultimately causes acute renal failure. AA3 inhibition is therefore a target of interest to prevent TCE induced nephrotoxicity. Here we report the crystal structure of recombinant mouse AA3 (mAA3) in the presence of its acetate byproduct and two substrates: N^{α}-acetyl-L-tyrosine and NA-DCVC. These structures, in conjunction with biochemical data, indicated that AA3 mediates substrate specificity through van der Waals interactions providing a dynamic interaction interface, which facilitates a diverse range of substrates.

mercapturates | metalloprotein | X-ray structure

Aminoacylase 3 (AA3) is a member of the aminoacylase family of enzymes that deacylates a broad range of substrates including both N^{α}-acetylated amino acids and *S*-cysteine conjugates of *N*-acetyl-L-cysteine (mercapturic acids) (Fig. 1) (1). There are three types of aminoacylases: (*i*) aminoacylase 1 (AA1) deacetylates neutral aliphatic *N*-acyl-α-amino acids and mercapturic acids; (*ii*) aminoacylase 2 or aspartoacylase (AA2) has a strict specificity for N^{α}-acetyl-L-aspartate (NAD); and (*iii*) aminoacylase 3 (AA3) preferentially deacetylates N^{α}-acetylated aromatic amino acids and mercapturic acids that are usually not deacetylated by AA1 (1–6). Despite different substrate specificities, AA2 and AA3 have a high degree of sequence (42% identity) and structure homology but are both substantially different from AA1 (~10% of sequence identity) (2, 6–10).

AA3 is of particular interest for human health because it participates in mediating toxicity of the xenobiotic trichloroethylene (TCE). The United States produces in excess of 130,000 tons of TCE per year (11), making it the most widespread chemical contaminant in both soil and ground water. TCE is readily absorbed into the body where it can enter the glutathione conjugation detoxification pathway producing the mercapturic acid *N*-acetyl-*S*-1,2-dichlorovinyl-L-cysteine (NA-DCVC) for subsequent urinary excretion (12, 13). However, NA-DCVC can be deacetylated by AA3—which is highly expressed in the renal proximal tubule, liver, and brain—to generate *S*-1,2-dichlorovinyl-L-cysteine (DCVC) (2) and further transformed via β-lyases or flavin monooxygenases into lethal products capable of causing acute renal failure and toxicity to the liver and brain. (4, 13–22). Thus, inhibition of AA3 can decrease DCVC formation and ameliorate TCE toxicity, presenting a potential target for drug discovery.

Generating specific inhibitors for AA3 would be greatly aided by high-resolution structural data, but structural studies of aminoacylases have been limited to AA1 (7) and AA2 (8, 9), which differ in both overall architecture and active site composition. For AA1, the active site has two cocatalytic zinc ions residing at the dimer interface (7). In contrast, the AA2 active site is formed within a single protein subunit comprising of a lone zinc ion at the active site (8, 9) and bears a striking similarity to carboxypeptidase A (CpA) (23). It is believed that both enzymes follow the "promoted-water pathway" mechanism for hydrolysis, where a zinc-bound hydroxide– generated by proton abstraction via a conserved glutamate– serves as the nucleophile to attack the substrate-leaving group (8, 9). Based on sequence identity (42%) and homology modeling, AA3 is believed to have a similar structure and mechanism for hydrolysis as AA2 (10). However, this model alone could not clarify the differences in substrate specificity between AA2 and AA3 (10). Therefore, an atomic resolution structure of AA3 in the presence of substrate is still required to address these questions and may facilitate targeted drug design.

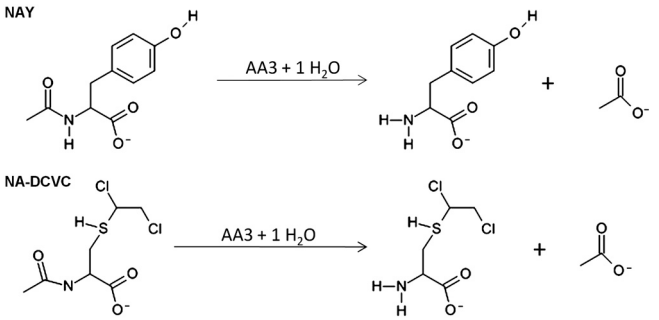

Fig. 1. Deacetylation reaction catalyzed by AA3. The AA3 substrate, *N*-acetyl-L-tyrosine (NAY), is hydrolyzed by AA3 to produce L-tyrosine and acetate. The AA3 substrate, *N*-acetyl-*S*-1,2-dichlorovinyl-L-cysteine (NA-DCVC), is hydrolyzed by AA3 to produce *S*-1,2-dichlorovinyl-L-cysteine (DCVC) and acetate.

Here we report the X-ray structure of murine AA3 (mAA3) (UniProt entry Q91XE4) in complex with the substrates N^{α}-acetyl-L-tyrosine (NAY) and *N*-acetyl-*S*-1,2-dichlorovinyl-L-cysteine (NA-DCVC). This feat was accomplished by mutating the essential glutamate residue (E177A) predicted to initiate the deacetylation reaction (8–10). Comparison of the wild-type (wt) mAA3 structure with the E177A-mAA3 structures in complex with substrate reveals key interactions involved in substrate binding. Further, a comparison with structures of AA2 highlights differences that facilitate the broad substrate recognition observed for AA3.

Author contributions: J.M.H., K.T., I.K., J.A., and A.P. designed research; J.M.H., K.T., N.M., and N.A. performed research; J.M.H., K.T., and M.R.S. analyzed data; and J.M.H., M.R.S., I.K., J.A., and A.P. wrote the paper.

The authors declare no conflict of interest.

*This Direct Submission article had a prearranged editor.

Data deposition: The atomic coordinates and structure factors have been deposited in the Protein Data Bank, www.pdb.org (PDB ID codes 3NH4, 3NFZ, 3NH5, and 3NH8).

[1]J.M.H. and K.T. contributed equally to this work.

[2]To whom correspondence may be addressed. E-mail: jabramson@mednet.ucla.edu or apushkin@mednet.ucla.edu.

This article contains supporting information online at www.pnas.org/lookup/suppl/doi:10.1073/pnas.1006687107/-/DCSupplemental.

Results

Structure of wt-mAA3. The wt-mAA3 crystals diffracted to 2.0 Å, and the data was phased by molecular replacement using rAA2 (PDB entry 2GU2) (8) as a search model. The model was built in COOT (24) and refined using PHENIX (25) with R_{work}/R_{free} of 18.4/20.7%. The data collection parameters and refinement statistics are presented in Table 1. All attempts to resolve the structure of wt-mAA3 in complex with known substrates failed. The initial structure determination of wt-mAA3 revealed a similar fold to AA2, and we identified a point mutation (E177A) rendering mAA3 catalytically inactive (10) but maintained the structural integrity of active site. The creation of E177A-mAA3 facilitated structure determination of mAA3 in complex with NAY (NAY-mAA3) and NA-DCVC (NA-DCVC-mAA3).

Structure Overview. A superposition of wt-mAA3 and rAA2 reveals similar architecture with a calculated rmsd of 1.04 Å over 298 C_α atoms. Similarly, no large conformational differences are observed among the four mAA3 structures reported here with rmsd values ranging from 0.267 to 0.349 Å, over 302 C_α atoms. There is one molecule per asymmetric unit (Fig. 2*A*); however, by applying a $P6_2$ symmetry operator the expected dimer is formed (Fig. 2*B*) as observed in the AA2 structures (8, 9) and is further substantiated by mAA3 biochemical data (26). The monomer is composed of two distinct domains, which have been predicted by trypsinolysis (26): the hydrolytic domain (residues 1–210), which maintains most of the essential residues for binding and hydrolysis; and the shielding domain (residues 211–318) that covers the active site to limit accessibility (Fig. 2).

A comparison of mAA3 with existing atomic resolution structures using the Distance ALIgnment (DALI) server (27) identified approximately five unique proteins (Z-score > 10) with similar structure including AA2; however, a notable inclusion was CpA, a pancreatic exopeptidase that hydrolyzes peptide bonds of C-terminal residues with aromatic or aliphatic side chains (sequence identity: 12.9%) (28). The two enzymes share a similar core of secondary structure elements in the hydrolytic domain with an overall structural alignment of 2.61 Å over 163 C_α atoms. Notably, CpA lacks the shielding domain and posses an N-terminal extension of approximately 60 residues. Nonetheless, the active site of these two enzymes reveals striking similarities where the essential mAA3 catalytic residues (His21, Glu24, Arg63, Asp68, His116, and Glu177) precisely conform to the active site residues of CpA (His69, Glu72, Arg127, Asp142, His196, and E270) (PDB ID 1CBX) (23). These six residues align with an rmsd of 0.352 Å (Fig. S1*A*), suggesting that AA3 and CpA use a similar reaction scheme for hydrolysis. Substantiating this claim, we examined the effects of the potent CpA inhibitor (L-benzylsuccinate) (23, 29) on mAA3, which resulted in inhibition of hydrolysis ($K_i = 25$ μM). This would suggest L-benzylsuccinate has a similar mode of interaction for both CpA and mAA3 further corroborating that AA3 uses the same reaction scheme as CpA.

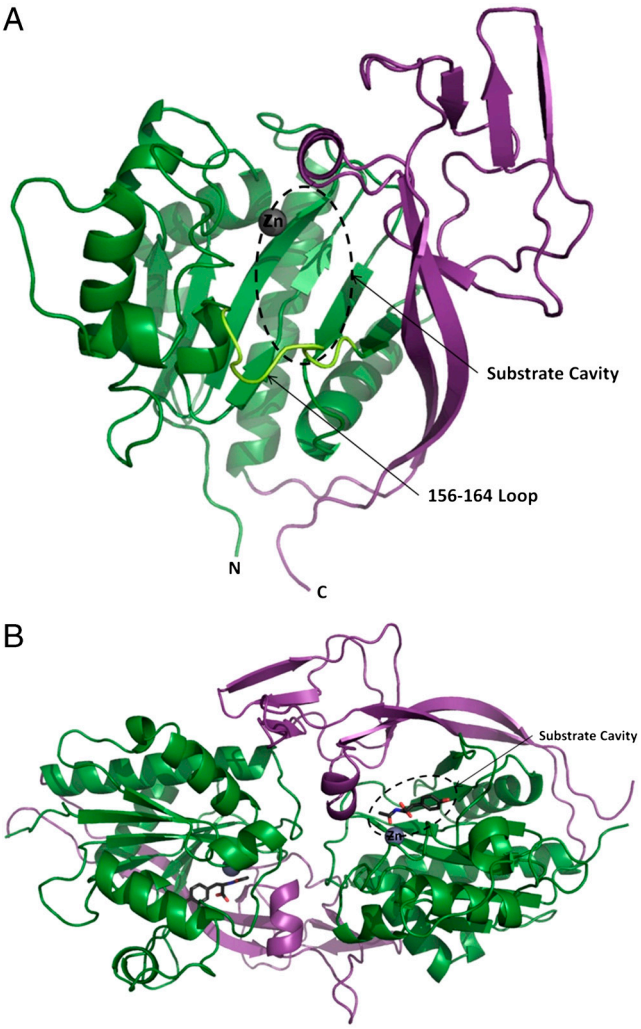

Fig. 2. Overview of mAA3 structure. (*A*) Single mAA3 protomer in ribbon representation with the substrate cavity and 156–164 loop indicated (light green). (*B*) Two mAA3 protomers form the biologically observed dimer with NAY substrate present. In both *A* and *B* the hydrolytic domain is colored green and the shielding domain is colored purple.

mAA3 with Acetate Byproduct. The essential catalytic residues of mAA3 (His21, Glu24, Arg63, Asp68, His116, and Glu177) are identical to those of AA2 and CpA. A zinc ion coordinated by

Table 1. Data collection and refinement statistics

	wt-mAA3	E177A-mAA3	NAY-mAA3	NA-DCVC-mAA3	Co^{2+} soaked wt-mAA3
Wavelength (Å)	0.9774	1.0000	1.0000	1.0000	1.2824
Spacegroup	$P6_2$	$P6_2$	$P6_2$	$P6_2$	$P6_2$
Unit Cell					
a, b, c (Å)	93.7, 93.7, 97.1	93.2, 93.2, 97.5	93.5, 93.5, 98.0	93.4, 93.4, 97.6	93.4, 93.4, 97.7
α, β, γ (°)	90, 90, 120	90, 90, 120	90, 90, 120	90, 90, 120	90, 90, 120
Resolution (Å)	50–2.00 (2.07–2.00)	50–2.10 (2.18–2.10)	50–2.15 (2.23–2.15)	50–2.80 (2.90–2.80)	50.0–2.80 (2.90–2.80)
R_{merge} (%)	6.4 (50.5)	9.2 (60.0)	12.2 (64.4)	15.4 (48.0)	11.0 (51.5)
Completeness (%)	100.0 (100.0)	98.6 (99.3)	100.0 (99.8)	98.2 (98.0)	98.8 (99.7)
Redundancy	4.9 (3.9)	6.8 (6.7)	6.7 (6.6)	4.2 (3.8)	6.7 (6.7)
I/σ	18.0 (3.0)	18.9 (2.6)	16.0 (3.4)	8.8 (2.2)	16.8 (4.0)
No. of Unique Reflections	32766 (3266)	27897 (2804)	26605 (2647)	11756 (1160)	11944 (1202)
R_{work}/R_{free}	18.4/20.7	19.4/22.7	16.6/19.7	17.5/22.4	—
rmsd					
Bonds (Å)	0.008	0.008	0.008	0.011	—
Angles (°)	1.038	1.035	1.038	1.470	—

His21, Glu24, and His116 is observed in all mAA3 structures. Previous studies have demonstrated that cobalt can replace zinc in the enzyme, and it increases enzymatic activity (6, 10)—a finding supported by "soaking" crystals in a cobalt solution revealing a mixed occupancy for both cobalt and zinc (confirmed by anomalous diffraction) (Fig. S2). The structures of wt-mAA3 and E177A-mAA3, crystallized in the presence of acetate and formate, reveal the reaction byproduct (acetate) coordinated in a bidentate fashion to the catalytic zinc. In addition, a formate molecule is observed coordinated to Arg63, Asn70, Arg71, and Tyr287 (Fig. 3*A*). A similar coordination pattern is observed to the *N*-acetyl group and α-carboxylate oxygens for both the NA-DCVC and NAY substrates (Fig. 3 *B* and *C*), suggesting a possible catalytic role for these residues.

Mutational analysis confirmed the importance of Arg63 and Tyr287 where the R63A substitution rendered the enzyme completely inactive while the Y287A mutation had minimal activity (8% for NAY and 2.5% for NA-DCVC) (10). In contrast, R71A and N70A had minimal effect on k_{cat} or affinity for both substrates (10). Strikingly, the R71K mutation cripples the human AA2 enzyme by reducing k_{cat} by approximately 95% without significant change of K_m (9), which indicates that that this residue plays quite different roles in AA2 as compared to AA3.

While both formate and acetate appear to mimic substrate binding, repeated attempts to solve the structure of wt-mAA3 in complex with known substrates proved unsuccessful. A comparative analysis with CpA highlights Glu177 as an essential residue for hydrolysis that when mutated to alanine renders AA3 inactive (10). In the wt-mAA3 Glu177 is coordinated to acetate, a byprodyct of deacetylation, highlighting its critical function. In the E177A-mAA3 mutant, this interaction is lost, but the overall structure and the coordination pattern to acetate and formate remains the same—a necessary requirement for structural analysis (Fig. S3).

NAY-Complex Structure. The E177A-mAA3 mutant was crystallized in the presence of NAY, which displaced both acetate and formate from the active site. The *N*-acetyl-α-amino carboxylic acid (NAACA) component of NAY—a conserved component of AA2 and AA3 substrates—is tightly bound by seven hydrogen bonds (Fig. 3*B*; see also Fig. S4 *A*, *B*). Specifically, the substrate's acetyl oxygen coordinates zinc and accepts two hydrogen bonds from Arg63; the α-carboxylic group forms a salt bridge with Arg71 and a hydrogen bond with Asn70; and the amide has hydrogen bonds to the hydroxyl of Tyr287. In addition, Tyr287 has van der Waals interactions with the NAACA component of NAY aiding in positioning the substrate.

The NAACA component of NAY has extensive hydrogen bonds and van der Waals interactions, but the side-chain constituent associates with AA3 primarily through van der Waals interactions and a lone hydrogen bond with Glu129. Eight residues maintain van der Waals contacts with the substrate side chain (Asn70, Arg71, Ile127, Glu129, Tyr156, Phe164, Ser165, Cys175) where five of these are conserved between human, rat, and mouse AA2 and AA3 (Asn70, Arg71, His116, Ile127, and Phe281) (6). This would indicate that these residues are likely not responsible for specificity between AA3 and the substrate side chain of NAY. The electron density for the 156–164 loop is not well defined for all structures reported here; however, the side-chain density for Tyr156 and Phe164 improves in the presence of NAY. Notably, in the presence of substrate, Phe164 rotates approximately 50° around the β-carbon to interact with NAY. A similar conformational rearrangement of the side chain of the homologous AA2 residue, Tyr164, was shown upon binding the intermediate analog, NPD (9). This data suggest a likely role for Phe164 in substrate recognition of NAY.

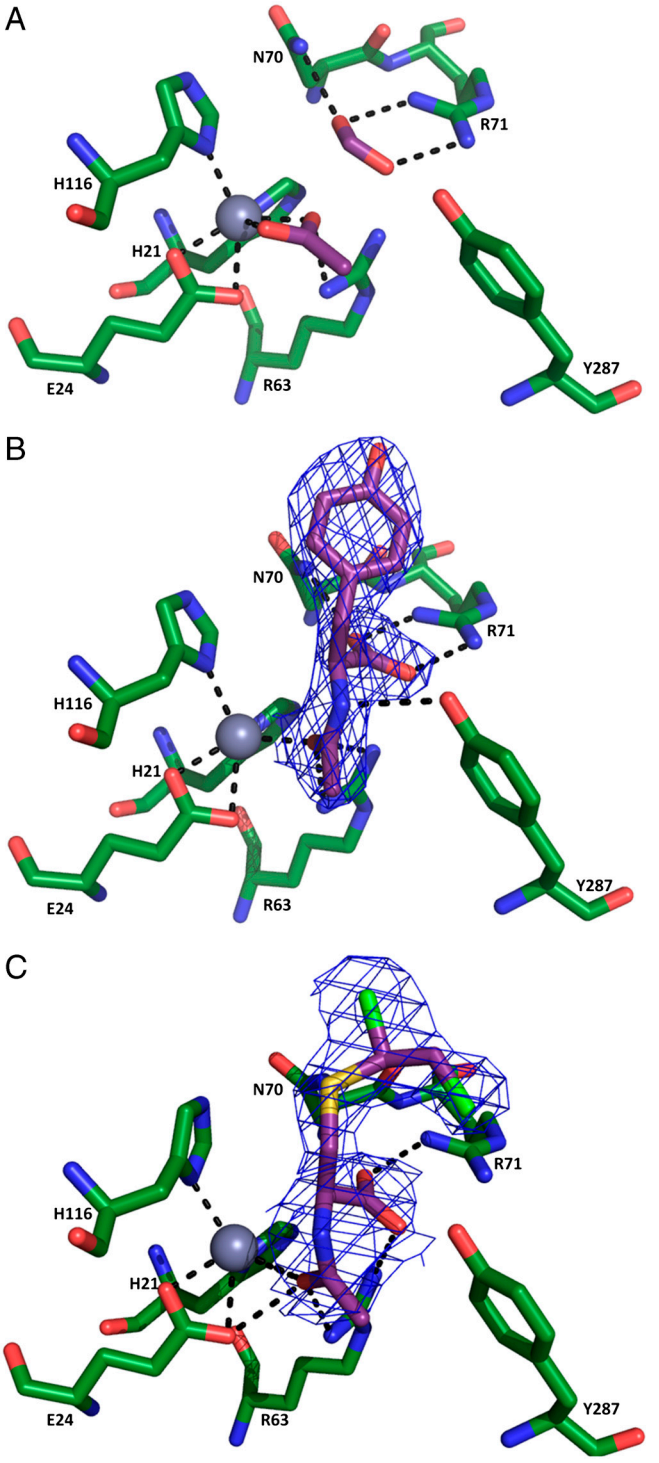

Fig. 3. mAA3 substrate binding. (*A*) wt-mAA3, with acetate and formate bound. (*B*) NAY-mAA3-E177A, with NAY bound in the active site. (*C*) NA-DCVC-mAA3-E177A, with NA-DCVC bound in the active site. The residues that form the hydrogen bonds with substrates and participate in the zinc ion (gray sphere) coordination are represented in green sticks, the molecules bound in the active site are purple and the hydrogen and coordination bonds are represented by dashed black lines. The $2F_o–F_c$ maps (in blue) are shown for both substrates, NAY and NA-DCVC, with a contour level of 1 and a carve radius of 1.6 and 1.8, respectively.

NA-DCVC-Complex Structure. E177A-mAA3 mutant crystals were soaked in 2 mM NA-DCVC to resolve the complex; further details regarding crystallization and structure determination can be found in *Materials and Methods*. Although similar to

the NAY structure, there is a 0.8 Å shift of the NAACA component causing a minor reorientation in the hydrogen-bonding network (Fig. 3*C*; see also Fig. S4 *C* and *D*). Specifically, the substrate's acetyl oxygen interacts with zinc and the side chains of Glu24 and Arg63. The α-carboxylic group accepts hydrogen bonds from the side chains of Arg71 and Tyr287, but unlike NAY-mAA3 there is no hydrogen bond with Asn70. The side-chain constituent of NA-DCVC interacts with AA3 solely through van der Waals interactions in a similar fashion as NAY with the exception of Phe164. Limited electron density for Phe164 suggests it is mostly disordered and does not undergo the 50° rotation observed in the NAY structure. These results suggest that AA3 has a more dynamic active site capable of accommodating a broad range of substrates.

Cavity Volume Measurements. AA3 typically hydrolyzes a broad range of *N*-acetylated bulky, aromatic amino acids and mercapturic acids, whereas AA2 solely hydrolyzes the smaller *N*-acetyl-L-aspartate (NAD) (1). A comparison of the previously published structures of AA2 (8, 9) and the mAA3 structures reported here provides a platform for analyzing substrate-specific binding. In the absence of substrate, the E177A-mAA3 cavity volume is 742.7 Å^3, and in the presence of substrate that volume marginally decreases (NAY volume is 649.6 Å^3 and NA-DCVC volume is 730.8 Å^3) (Fig. 4 *A* and *B*). For AA2, in the absence of substrate, the human AA2 cavity volume is 630.3 Å^3 (PDB ID: 2O53), and in the presence of the inhibitor, NPD (PDB ID: 2O4H), it is dramatically reduced to 394 Å^3 (Fig. 4*C*), primarily through a rearrangement of the 156–164 loop. Unlike AA3, there is a large decrease in AA2 cavity volume indicative of a specific arrangement for substrate recognition, which is not observed in AA3.

Amino Acids that Affect Catalysis and Specificity. Residues His21, Glu24, Arg63, Asp68, His116, and Glu177 are essential for activity (10). Glu177, hypothesized to activate the nucleophilic water molecule, results in complete inactivation when mutated to an alanine (E177A). However, the more mild mutation to aspartate (E177D) reduces the k_{cat} more than threefold (0.3 s^{-1}) suggesting the side-chain length is imperative for maximal activity. Another primary residue, Tyr287, appears to position the NAACA component of the substrate, and a mutation to alanine (Y287A) greatly diminishes k_{cat} for both NAY (~8% of wt-mAA3 k_{cat}) and NA-DCVC (~2.5% of wt-mAA3 k_{cat}), further supporting this hypothesis (10). Arg71, Tyr156, Phe164 interact with the substrate but have only a modest affect on activity when mutated to alanine. Specifically, R71A and F164A resulted in an approximately 2.0-fold increase in k_{cat}, while Y156A decreases k_{cat} by 1.3-fold with respect to wt-mAA3. Although these residues are not essential for hydrolysis, these findings confirm a contribution and further highlight their role in substrate recognition and hydrolysis, which are not mutually exclusive.

Human AA2—in complex with NPD—shows Arg168 forming a salt bridge to the carboxylic acid side chain of NPD, and even the most mild mutation, R168K, nearly abolishes activity (9). In contrast, wt-mAA3 is unable to hydrolyze the AA2 substrate (NAD), which is likely due to the absence of a positively charged residue at position 167. The corresponding residue in mAA3 is Glu167 pointed away from the substrate cavity. To test this hypothesis, the E167R-mAA3 mutant was checked for NAD hydrolysis and exhibited a k_{cat} of 0.1 s^{-1} (~10% of wt-AA3 with NAY). The E167R-mAA3 mutant also hydrolyzed NAY but at a decreased rate (k_{cat} 0.6 s^{-1}), suggesting that—unlike AA2—the residue at position 167 is not the sole factor involved in substrate specificity.

Discussion

AA3 is an important component of the biochemical mechanism that leads to acute renal failure induced by the common environmental contaminant TCE. It is generally accepted, that the nephrotoxicity of TCE is mediated by the deacetylation product of NA-DCVC, which is further, transformed into toxic compounds by β-lyases or flavin monooxygenases (12, 30). Several enzymatic steps lead to the formation of these toxic products, but these enzymes are members of large groups of ubiquitously expressed proteins, in which specific inhibition would be unlikely, leading to adverse side effects (31–34). Thus, AA3 represents an attractive target to eliminate TCE toxicity due to its restricted expression pattern and absence of multiple isoforms (2, 3).

Our study reveals strong similarities in the reaction mechanisms of AA3, CpA, and AA2 and further demonstrates parallels in the active site constituents for binding the substrate NAACA component. The unique aspect of this study is that it generates previously undescribed insights into the structural determinants for different substrate specificity of AA3 and provides the platform for generating specific inhibitors of AA3. Comparison of AA3 and AA2 crystal structures shows that AA3's specificity is primarily mediated through van der Waals interactions with the substrate's side chain.

Upon substrate binding, the electron density for Tyr156 and Phe164 became more resolved, suggesting these residues are likely involved in substrate specificity. mAA3 is capable of hydrolyzing a variety of different substrates with varying side-chain lengths ranging from 7.2 to 11 Å (Cα to the terminal side-chain atom) (6) but is not capable of hydrolyzing the smaller AA2 substrate NAD (4.5 Å in length). This broad specificity can be partially attributed to the limited mobility of the loop formed by residues 156–164 (Fig. S1*B*). In contrast, the AA2 loop is very mobile (shift of 10 Å) and Tyr164 rotates approximately 45° around the Cα-Cβ bond, causing a dramatic reduction in sub-

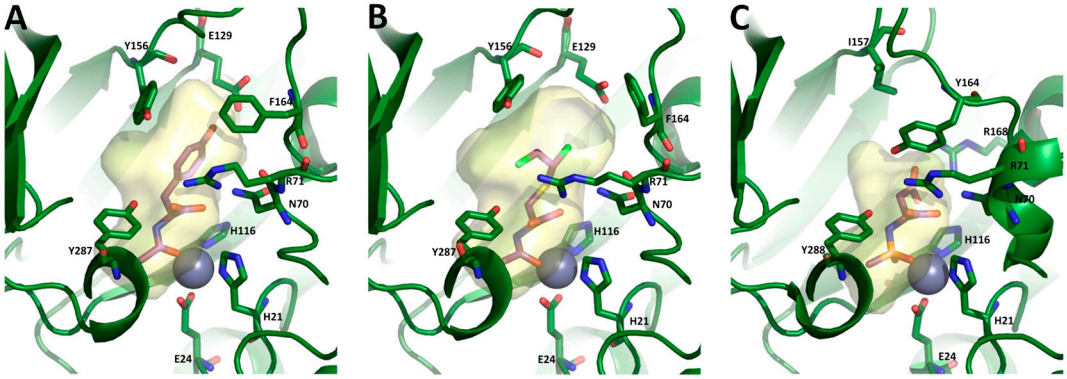

Fig. 4. Aminoacylase substrate cavity. (*A*) NAY-mAA3, cavity volume is 649.6 Å^3; (*B*) NA-DCVC-mAA3, cavity volume is 730.8 Å^3; and (*C*) human AA2 with NPD bound, cavity volume is 394.0 Å^3. The residues forming the cavity have been highlighted as sticks. For human AA2, R168 and the corresponding residues to mAA3 are highlighted in green sticks. The substrate/inhibitor molecule is in purple and the cavity space is highlighted as a transparent yellow surface.

strate cavity for substrate-bound human AA2 (~395 Å^3); in comparison in mAA3, the substrate cavity with NA-DCVC and NAY is approximately 730 and 650 Å^3, respectively. The differences in loop dynamics could be attributed to the sequence divergence observed between the AA2 and AA3 loops (6).

One of the important differences between AA2 and AA3, contributing to AA2 substrate specificity, is Arg168, which stabilizes the AA2 inhibitor analog NPD through a salt bridge. Even the mild mutation of R168K nearly abolishes activity (9). mAA3 has a glutamate at this position, and its mutation to an alanine did not significantly change the enzyme kinetics (10). It is interesting that the E167R-mAA3 mutant, contrary to wt-AA3, demonstrated limited NAD hydrolysis ($k_{cat} \sim 10\%$ and 20% of, respectively, the wt-AA3 and E167R mutant k_{cat} with NAY). Although, these data demonstrate some similarity between AA3 and AA2, they also highlight specific differences in active site architecture.

As seen in the AA3 structures, residues His21, Glu24, and His116 are responsible for coordinating the zinc involved in catalysis. Substrate binding is modulated through the substrate's NAACA component where residues His21, Glu24, Arg63, and Tyr287 interact via hydrogen bonding and van der Waals interactions (Fig. 3 *B* and *C*). His21, Glu24, Arg63, and Tyr288 also play a similar role in AA2. For AA2, Arg71 is an essential residue for positioning the substrate NAACA component via hydrogen bonds, and Arg71 mutation even into lysine decreases k_{cat} by 99% (9); however, it is not the case for AA3, in which the efficiency of catalysis is not significantly affected by the R71A mutation (10). Instead, AA3 uses Tyr287, located on the shielding domain, for positioning substrate in the active site via van der Waals interactions. Tyr287 is conserved among AA2 and AA3, and the Y287A mutant of mAA3 experiences a large drop in activity (10), further supporting the importance of this residue. Furthermore, Asn70 that participates in positioning of the substrate NAACA component in AA2 (8, 9) similar to Arg71 does not play a significant role in AA3 (10).

The four mAA3 structures presented here have provided insight into the mechanism of substrate binding and begin to explain the substrate specificity observed. The data indicate that AA3 and AA2 use a similar mechanism for binding the substrate's NAACA component, but further analysis revealed certain structural differences that are responsible for substrate specificities. This data form the basis for generating specific inhibitors of AA3 to use for protection from TCE and similar environmental contaminants.

Materials and Methods

Expression and Purification of mAA3. wt-mAA3 and mutants were expressed in *Escherichia coli* using the pRSET vector (Invitrogen, Carlsbad, CA) containing an N-terminal Strep(II)-tag. The sequence of the construct was confirmed by bidirectional sequencing using an ABI 310 sequencer (Perkin Elmer, Foster City, CA). *E. coli* cells were grown to an optical density of 0.6 and then induced with 1 mM isopropyl β-D-thiogalactopyranoside for 3 h. After harvesting, cells were washed with PBS and lysed in BugBuster HT Protein Extraction Reagent (Novagen, Madison, WI) supplemented with a complete protease inhibitor cocktail (Roche, Indianapolis, IN), centrifuged (40,000 g, 30 min), and the supernatant was loaded onto a 5 ml StrepTactin Sepharose column (GE Healthcare, Piscataway, NJ). The column was washed with 50 mM Tris-HCl buffer, pH 7.5, containing 150 mM NaCl, and eluted with 3 mM desthiobiotin (Sigma, Milwaukee) in the same buffer. Desthiobiotin was removed from the eluate using a PD-10 desalting column (GE Healthcare). The purity of mAA3 in the final preparation was >99% as estimated by SDS/PAGE in which protein bands were visualized with Coomassie brilliant blue R250 (Sigma).

Active Site Mutants and Kinetic Studies. mAA3 mutants with substitutions E167R, E177D, and C175A were made using the QuickChange site-directed mutagenesis kit from Stratagene (La Jolla, CA). Sequences of all constructs were confirmed via bidirectional sequencing using an ABI 310 sequencer (Perkin Elmer, Foster City, CA).

Activity of wt-mAA3 and mutants was determined with NAY, NA-DCVC, and NAD by measuring the deacetylated product in a fluorescence assay in the presence of 0.1 mM $CoCl_2$ (6, 35). The calibration curves were made with L-tyrosine, DCVC, and L-aspartate. The experiments were performed in at least triplicate. The K_m and k_{cat} values were calculated by fitting data to the Michaelis–Menten equation using the OriginPro 7.5 software (OriginLab Corp., Northampton, MA). All values are means ± S.E. of measurements of at least three separate experiments.

Crystal Growth and Structure Determination. Purified wt-mAA3 or E177A-mAA3 protein was maintained in a solution of 50 mM Tris, pH 7.5, and 150 mM NaCl at a concentration of 10 mg/ml. This solution was screened for crystallization against a number of commercially available screens using the mosquito crystallization robot (TTP Labtech) and the hanging drop vapor diffusion technique. The crystals were obtained at 20 °C in 2 M sodium formate and 0.1 M sodium acetate, pH 5.0. The wt-mAA3 crystal was optimized further using Hampton Research's Additive Screen where 0.1 M cesium chloride improved the quality of the crystal diffraction. The E177A mutant with NAY (NAY-mAA3) crystals were obtained by cocrystallizing in formate/acetate with 2 mM NAY in the drop. These three crystal types were cryoprotected by adding 1 μl of 2 M sodium formate, 0.1 M sodium acetate, pH 5.0, and 50% glycerol to the drop. The NA-DCVC+E177A-mAA3 crystals were obtained in 15% PEG 4000 and 0.1 M Na cacodylate, then cryoprotected by adding 1 μl of 15% PEG 4000, 0.1 M Na cacodylate, 20% glycerol, and 2 mM NA-DCVC to the drop and immediately freezing the crystals. NA-DCVC and DCVC were synthesized and characterized as previously described (10).

Data were collected from cryocooled crystals at beamlines 5.0.1 (wt-mAA3) and 5.0.2 (E177A-mAA3, NAY-mAA3, and NA-DCVC-mAA3) of the Advance Light Source (Berkeley, CA). All crystals belong to the space group $P6_2$ with average cell dimensions of $a = 93.5$ Å, $b = 93.5$ Å, $c = 97.5$ Å; exact values for each can be found in Table 1. Image data were processed using the programs DENZO and SCALEPACK (36). The structure of wt-mAA3 was phased by molecular replacement using the program PHASER (37, 38) where the coordinates of the rat AA2 structure (PDB accession code 2GU2) were used as the search model (8). Model building was done using the program COOT (24) and refinement was carried out using PHENIX (25).

The NAY and NA-DCVC molecules were initially built using the program SKETCHER (a module in CCP4i) (38) and refined based on experimental data of the NAY+E177A-mAA3 and NA-DCVC+E177A-mAA3 structures, respectively.

Cobalt Anomalous Data Collection. wt-mAA3 crystals were grown as described above and then soaked in the formate and acetate crystallization solution containing 6 mM $CoCl_2$ for 1 h and then back soaked for 30 min to remove excess Co^{2+}. The crystals were cryoprotected as described above. Data were collected from cryocooled crystals at beamline 5.0.2 of the Advance Light Source (Berkeley, CA) at λ-1.2824 Å. Image data were processed using the programs DENZO and SCALEPACK (36) and the anomalous difference Fourier map was calculated using the CCP4 program suite (38).

ACKNOWLEDGMENTS. The authors wish to thank the Advance Light Source (P. Zwart and beamline staff at 5.0.1 and 5.0.2). This work was supported by the National Institutes of Health Grant R01 ES012935 (A.P.) and R01 GM078844 and R21 HL093278 (J.A.).

1. Anders M, Dekant W (1994) Aminoacylases. *Adv Pharmacol* 27:431–448.
2. Pushkin A, et al. (2004) Structural characterization, tissue distribution, and functional expression of murine aminoacylase III. *Am J Physiol-Cell Ph* 286(4):C848–C856.
3. Uttamsingh V, Keller DA, Anders MW (1998) Acylase I-catalyzed deacetylation of *N*-acetyl-L-cysteine and *S*-alkyl-*N*-acetyl-L-cysteines. *Chem Res Toxicol* 11(7):800–809.
4. Uttamsingh V, Anders MW (1999) Acylase-catalyzed deacetylation of haloalkene-derived mercapturates. *Chem Res Toxicolol* 12(10):937–942.
5. Le Coq J, An HJ, Lebrilla C, Viola RE (2006) Characterization of human aspartoacylase: The brain enzyme responsible for Canavan disease. *Biochemistry* 45(18):5878–5884.
6. Newman D, et al. (2007) Specificity of aminoacylase III mediated deacetylation of mercapturic acids. *Drug Metab Dispos* 35(1):43–50.
7. Lindner HA, et al. (2003) Essential roles of zinc ligation and enzyme dimerization for catalysis in the aminoacylase-1/M20 family. *J Biol Chem* 278(45):44496–44504.
8. Bitto E, Bingman CA, Wesenberg GE, McCoy JG, Phillips GN (2007) Structure of aspartoacylase, the brain enzyme impaired in Canavan disease. *Proc Natl Acad Sci USA* 104(2):456–461.
9. Le Coq J, et al. (2008) Examination of the mechanism of human brain aspartoacylase through the binding of an intermediate analogue. *Biochemistry* 47(11):3484–3492.
10. Tsirulnikov K, et al. (2009) Mouse aminoacylase 3: A metalloenzyme activated by cobalt and nickel. *Biochim Biophys Acta* 1794(7):1049–1057.
11. DeRosa CT, Johnson BL, Fay M, Hansen H, Mumtaz MM (1996) Public health implications of hazardous waste sites: Findings, assessment and research. *Food Chem Toxicol* 34(11–12):1131–1138.

12. Birner G, Bernauer U, Werner M, Dekant W (1997) Biotransformation, excretion and nephrotoxicity of haloalkene-derived cysteine *S*-conjugates. *Arch Toxicol* 72:1–8.
13. Dekant W, Vamvakas S, Anders M (1994) Formation and fate of nephrotoxic and cytotoxic glutathione *S*-conjugates: Cysteine conjugate β-lyase pathway. *Adv Pharmacol* 27:114–162.
14. Silber PM, Gandolfi AJ, Brendel K (1986) Early biological indicators of *S*-(1,2-dichlorovinyl)-L-cysteine nephrotoxicity in the rabbit. *Drug Chem Toxicol* 9(3–4):285–303.
15. Wolfgang GHI, Gandolfi AJ, Stevens JL, Brendel K (1989) *N*-acetyl *S*-(1,2-dichlorovinyl)-L-cysteine produces a similar toxicity to *S*-(1,2-dichlorovinyl)-L-cysteine in rabbit renal slices—differential transport and metabolism. *Toxicol Appl Pharmacol* 101(2):205–219.
16. Wallin A, Zhang GH, Jones TW, Jaken S, Stevens JL (1992) Mechanism of the nephrogenic repair response—studies on proliferation and vimentin expression after ^{35}S-1,2-dichlorovinyl-L-cysteine nephrotoxicity in vivo and in cultured proximal tubule epithelial-cells. *Lab Invest* 66(4):474–484.
17. Kays SE, Berdanier CD, Swagler AR, Lock EA, Schnellmann RG (1993) An in-vitro model of renal proximal tubule cell regeneration. *J Pharmacol Toxicol Methods* 29(4):211–215.
18. Cooper A (1994) Enzymology of cysteine *S*-conjugate beta-lyases. *Adv Pharmacol* 27:71–113.
19. Lash LH, Putt DA, Parker JC (2006) Metabolism and tissue distribution of orally administered trichloroethylene in male and female rats: Identification of glutathione- and cytochrome P-450-derived metabolites in liver, kidney, blood, and urine. *J Toxicol Env Health A* 69(13):1285–1309.
20. Anders MW, Dekant W (1998) Glutathione-dependent bioactivation of haloalkenes. *Annu Rev Pharmacol Toxicol* 38:501–537.
21. Bull RJ (2000) Mode of action of liver tumor induction by trichloroethylene and its metabolites, trichloroacetate and dichroloacetate. *Environ Health Persp* 108(Suppl 2): 241–259.
22. Barton HA, Clewell HJ, III (2000) Evaluating noncancer effects of trichloroethylene: dosimetry, mode of action, and risk assesment. *Environ Health Persp* 108(Suppl 2): 323–334.
23. Mangani S, Carloni P, Orioli P (1992) Crystal-structure of the complex between carboxypeptidase A and the biproduct analog inhibitor L-benzylsuccinate at 2.0 Å resolution. *J Mol Biol* 223(2):573–578.
24. Emsley P, Cowtan K (2004) Coot: Model-building tools for molecular graphics. *Acta Crystallogr D* 60:2126–2132.
25. Adams PD, et al. (2010) PHENIX: A comprehensive Python-based system for macromolecular structure solution. *Acta Crystallogr D* 66:213–221.
26. Ryazantsev S, et al. (2007) Structural characterization of dimeric murine aminoacylase III. *FEBS Lett* 581(9):1898–1902.
27. Holm L, Kaariainen S, Rosenstrom P, Schenkel A (2008) Searching protein structure databases with DaliLite v.3. *Bioinformatics* 24(23):2780–2781.
28. Christianson DW, Lipscomb WN (1989) Carboxypeptidase A. *Accounts Chem Res* 22(2):62–69.
29. Byers LD, Wolfende R (1973) Binding of by-product analog benzylsuccinic acid by carboxypeptidase A. *Biochemistry* 12(11):2070–2078.
30. Dekant W, Martens G, Vamvakas S, Metzler M, Henschler D (1987) Bioactivation of tetrachloroethylene. Role of glutathione *S*-transferase-catalyzed conjugation versus cytochrome P-450-dependent phospholipid alkylation. *Drug Metab Dispos* 15(5):702–709.
31. Lebrun P, Malaisse WJ, Herchuels A (1983) Impairment by aminoaxiacetate of ionic response to nutrients in pancreatic islets. *Am J Physiol-Endoc M* 245:E38–E46.
32. Guth PS, et al. (1990) Evaluation of amino-oxyacetic acid as a palliative in tinnitus. *Ann Oto Rhinol Laryn* 99:74–79.
33. Kurozumi Y, Abe T, Yao W-B, Ubuka T (1999) Experimentyal β-alaninuria induced by (aminooxy)acetate. *Acta Med Okayama* 53:13–18.
34. Subramanian RK, et al. (2007) Reassessment of the mechanism by which aminoaxyacetate (AOA) inhibits gluconeogenesis (GNG) from lactate. *FASEB J* 21:804.1.
35. Udenfriend S, et al. (1972) Fluorescamine—reagent for assay of amino-acids, peptides, proteins, and primary amines in picomole range. *Science* 178(4063):871–872.
36. Otwinowski Z, Minor W (1997) Processing of X-ray diffraction data collected in oscillation mode. *Method Enzymol*, eds CW Carter, Jr and RM Sweet (Academic, San Diego), 276, pp 307–326.
37. McCoy AJ, et al. (2007) Phaser crystallographic software. *J Appl Crystallogr* 40:658–674.
38. Collaborative Computational Project N (1994) The CCP4 suite: Programs for protein crystallography. *Acta Crystallogr D* 50(5):760–763.